Research Square

Preprints are preliminary reports that have not undergone peer review.
They should not be considered conclusive, used to inform clinical practice,
or referenced by the media as validated information.

Multidecadal and Multi-seasonal Dynamics of Urban Heat in Chicago (1992-2023)

Samanta Alam
Chicago State University
Anil Bhattarai
Chicago State University
Abigiya Haile
Chicago State University
TEKLEAB GALA
tgala@csu.edu

Chicago State University
Daniel Block
Chicago State University

Research Article

Keywords: Urban Heat, Land Surface Temperature (LST), Remote Sensing, Climate Change, Chicago

Posted Date: July 7th, 2026

DOI: https://doi.org/10.21203/rs.3.rs-9579900/v1

License: This work is licensed under a Creative Commons Attribution 4.0 International License.
Read Full License

Additional Declarations: No competing interests reported.

Abstract

Urban heat has emerged as a significant environmental and public health concern in rapidly urbanizing regions, driven by the combined effects of land-use transformation and global climate change. This study investigates the long-term spatiotemporal dynamics of urban heat in Chicago, Illinois, over a 31-year span (1992–2023) using multitemporal Landsat imagery. The approach involved developing and integrating land surface temperature (LST), the vegetation index (NDVI), and the built-up area index (NDBI) to assess the evolution of urban thermal patterns and identify key drivers of observed changes. The findings reveal persistent spatial disparities in Chicago's LST landscape, underscoring important environmental justice issues and the need for targeted interventions. Temporally, mid-summer LST values are consistently higher than late-summer values, with significant interannual variability during extreme heat years. Despite increases in vegetation cover and reductions in built-up intensity, LST has increased across Chicago, suggesting that rising ambient air temperatures are attributable to broader climatic shifts, which may contribute to the escalation of urban heat. Consequently, effective UHI mitigation strategies for Chicago may require coordinated, integrated, and multi-scalar approaches to foster a thermally sustainable urban environment.

1. Introduction

Urban heat has become a major environmental and public health concern worldwide, particularly in rapidly urbanizing cities where land-use changes and climate change interact to intensify thermal conditions (IPCC, 2021; Li et al., 2019). The Urban Heat Island (UHI) effect, in which urban areas experience significantly higher temperatures than surrounding rural regions, is primarily driven by the expansion of impervious surfaces, reduced vegetation, and increased anthropogenic heat emissions (Aghazadeh et al., 2025; Li et al., 2019; Morabito et al., 2021; Zhou et al., 2014). These transformations increase heat absorption and storage while limiting natural cooling processes such as evapotranspiration, resulting in elevated land surface temperatures (LST) and intensified urban heat (Weng et al., 2009; Zhou et al., 2014; Ziter et al., 2019). In addition, urban design characteristics such as dense building configurations and street canyon effects restrict airflow and amplify heat retention, while meteorological and geographic factors, including wind patterns, cloud cover, and proximity to water bodies, further influence the spatial variability and intensity of urban heat (Lokoshchenko & Alekseeva, 2023; Santamouris, 2015). Anthropogenic heat emissions from transportation, industrial activities, and energy consumption further intensify urban thermal environments (Sailor, 2011; Shahmohamadi et al., 2011).

The effects of intensified urban heat are substantial and multifaceted. Environmentally, elevated temperatures disrupt thermal comfort, degrade air quality, and alter local microclimates (Grimmond & Oke, 1999; IPCC, 2021; Pawlowski et al., 2026). They also increase emissions of greenhouse gases and aerosols, establishing feedback mechanisms that further intensify climate change. From a public health perspective, extreme heat events are associated with higher mortality, heat stress, related illnesses, and heightened vulnerability among older adults and low-income populations (Anderson & Bell, 2010; Ebi et

al., 2021; Pawlowski, 2025). Socioeconomically, urban heat contributes to higher energy consumption and healthcare costs, strained infrastructure, and reduced worker productivity (Estrada et al., 2017; Im et al., 2017; Perkins-Kirkpatrick & Gibson, 2017).

Recent studies emphasize that the urban heat island (UHI) effect also raises environmental justice concerns, as marginalized communities often face disproportionately higher heat exposure and associated hazards due to unequal access to green spaces and cooling infrastructure (Hoffman et al., 2020; Tan et al., 2023). High-resolution urban temperature studies in Chicago further demonstrate that these inequalities are spatially embedded, showing that ethnic minority and low-income communities experience significantly higher land surface temperatures than predominantly White neighborhoods. This pattern highlights the intersection of urban heat, gentrification, and environmental inequality (Alfraihat et al., 2016; Sampson et al., 2013; Lee et al., 2024). Other studies have examined the relationship between urban heat dynamics and land-surface characteristics in Chicago (Li et al., 2019; Weng et al., 2009; Zhou et al., 2014). Despite the city's expanding implementation of mitigation strategies such as urban greening, reflective surfaces, and enhanced urban planning (Chun & Guldmann, 2018; Fadhil et al., 2023; Tan et al., 2023), recent evidence indicates that the intensity of urban heat continues to increase steadily (Chen et al., 2023; Zhou et al., 2017).

Chicago's pivotal case for analyzing UHI dynamics stems from the 1995 Chicago Heat Wave, which exposed significant environmental and social vulnerabilities across the city (Semenza et al., 1999; Klinenberg, 2002; Wuebbles et al., 2021). Recent climate assessments indicate that the region has warmed over the past century, with more frequent extreme heat events, and projections point to continued warming and heightened heat risks (IPCC, 2021; Wuebbles et al., 2021; Janků et al., 2024). With an estimated population of 2.72 million, Chicago is the third-largest city in the United States and the largest in the Midwest (U.S. Census Bureau, 2023), underscoring the need for further inquiry. Nearly 17% of Chicago's urban region is covered by vegetation, including ground cover and tree canopy, while paved surfaces account for 31% and buildings make up approximately 27% of the urban landscape (Friehat et al., 2015; Smith et al., 2026; U.S. Environmental Protection Agency, 2002). Chicago's continental climate, with particularly hot summers, means that peak temperatures in July and August often exceed 35°C, underscoring the need to examine urban heat in the city. Previous studies are often limited to short-term analyses or specific time periods and provide inconclusive assessments of long-term spatiotemporal trends and the combined influence of land-cover change and broader climatic variability over multiple decades.

Therefore, this study analyzes long-term trends in land surface temperature (LST) in Chicago from 1992 to 2023 and evaluates how urban heat patterns have changed over time. Additionally, the study explores the relationship between observed temperature fluctuations and broader climatic and environmental conditions and identifies areas within the city that are persistently prone to heat accumulation. A multi-temporal remote sensing and GIS-based analytical framework is employed to provide consistent, spatially explicit observations of urban thermal conditions. By integrating vegetation, built-up, and thermal indices with observed air temperature data, the study provides a comprehensive assessment of

urban heat dynamics and their drivers. This approach has been used in several studies for land surface temperature inversion and subsequent investigations of the urban heat island (e.g., Zhou et al., 2017; Lokoshchenko & Alekseeva, 2023; Lee et al., 2024).

2. Materials and Methods

2.1. Research data source, Acquisition, and Pre-processing

For over four decades, the Landsat satellite series has provided the most extensive continuous record of space-based observations of Earth's surface. Data from these satellites have been widely used for mapping and monitoring land cover and for evaluating biophysical and geophysical surface properties (e.g., Habila, 2018; Boakye, 2019; Mengisti et al., 2021). These data have also been applied to terrestrial modeling, biogeochemical cycles, and land-use forecasting (Lewis et al., 2012; McKenzie, 2022; McKenzie & Gala, 2023). For this study, data from the Landsat 5 Thematic Mapper (TM), Landsat 7 Enhanced Thematic Mapper Plus (ETM+), and Landsat 8 Operational Land Imager (OLI) combined with the Thermal Infrared Sensor (TIRS) were acquired via the USGS Earth Explorer platform. These sensors record data across visible, near-infrared, shortwave infrared, and thermal infrared spectral bands, with a spatial resolution of 30 meters for multispectral data and 60–100 meters for thermal bands. The thermal infrared bands are particularly important for estimating land surface temperature (LST), while the multispectral bands facilitate the computation of vegetation indices (e.g., NDVI) and built-up indices (e.g., NDBI). The historical Landsat archive is used to analyze long-term trends in land surface temperature (LST) and its drivers in Chicago. Table 1 presents the specifications of the multitemporal satellite data used in this study.

Table 1
Specification of Multitemporal Landsat data

Date	Acquisition Time (Local)	Sensor	Path/Row	Spectral Resolution	Cloud Cover (%)	Season
09-10-1992	15:57:02–15:57:29	Landsat 5 TM	023/031	7 bands	0	Late Summer
07-01-1995	15:40:20–15:40:47	Landsat 5 TM	023/031	7 bands	1	Mid-Summer
08-29-2005	16:22:58–16:23:25	Landsat 5 TM	023/031	7 bands	1	Late Summer
07-15-2006	16:27:55–16:28:22	Landsat 5 TM	023/031	7 bands	0	Mid-Summer
07-21-2014	16:34:42–16:35:14	Landsat 8 OLI/TIRS	023/031	11 bands	0.52	Mid-Summer
09-23-2014	16:34:55–16:35:26	Landsat 8 OLI/TIRS	023/031	11 bands	0.04	Late Summer
07-14-2023	16:34:32–16:35:04	Landsat 8 OLI/TIRS	023/031	11 bands	3.09	Mid-Summer
08-31-2023	16:34:49–16:35:21	Landsat 8 OLI/TIRS	023/031	11 bands	0.16	Late Summer

To analyze seasonal variability in the urban heat phenomenon, images were carefully selected for the mid-summer and late-summer periods. Mid-summer imagery comprised data from 1995, 2006, 2014, and 2023, whereas late-summer imagery included data from 1992, 2005, 2014, and 2023. For quality assurance, only images with less than 5% cloud cover were used. All Landsat images underwent preprocessing in ArcGIS Pro, including atmospheric correction, reprojection, and georectification. Hourly air temperature data were obtained from the Midway Airport station via Weather Underground. Only measurements taken within ± 2 hours of the Landsat overpass were considered and averaged over that period. These ambient air temperature data were used to validate the relationship between land surface temperature derived from Landsat imagery and atmospheric temperature records. Table 2 presents the specifications of the ambient atmospheric temperature data used in this study.

Table 2
Specification of ambient atmospheric temperature at the time of satellite overpass

Date	Station	Landsat Overpass Time	Air Temperature Window Used	Variable
09-10-1992	Midway Airport	15:57:02–15:57:29	2:00 pm – 6:00 pm	Air Temp (°C)
07-01-1995	Midway Airport	15:40:20–15:40:47	2:00 pm – 6:00 pm	Air Temp (°C)
08-29-2005	Midway Airport	16:22:58–16:23:25	2:00 pm – 6:00 pm	Air Temp (°C)
07-15-2006	Midway Airport	16:27:55–16:28:22	2:00 pm – 6:00 pm	Air Temp (°C)
07-21-2014	Midway Airport	16:34:42–16:35:14	2:00 pm – 6:00 pm	Air Temp (°C)
09-23-2014	Midway Airport	16:34:55–16:35:26	2:00 pm – 6:00 pm	Air Temp (°C)
07-14-2023	Midway Airport	16:34:32–16:35:04	2:00 pm – 6:00 pm	Air Temp (°C)
08-31-2023	Midway Airport	16:34:49–16:35:21	2:00 pm – 6:00 pm	Air Temp (°C)

2.2. Calculation Indices

2.2.1. Normalized Difference Vegetation Index

The Normalized Difference Vegetation Index (NDVI) is a metric used in remote sensing to assess vegetation health and canopy cover across the landscape. This index utilizes the differential reflectance properties of the near-infrared (NIR) and red spectral bands in satellite imagery as they interact with vegetated land surfaces. Table 3 summarizes the spectral characteristics of the bands involved.

Table 3
Landsat spectral bands used for NDVI calculation

Landsat Sensor	NIR Band	Red Band	Wavelength Range (nm)
Landsat 5 TM	Band 4	Band 3	NIR: 760–900; Red: 630–690
Landsat 7 ETM+	Band 4	Band 3	NIR: 770–900; Red: 630–690
Landsat 8 OLI	Band 5	Band 4	NIR: 850–880; Red: 630–680
NDVI is given by:			

$$NDVI = \frac{NIR - RED}{NIR + RED}$$ (Eq. 1)

where NIR and RED represent the reflectance values of the near-infrared and red bands, respectively. NDVI ranges from − 1 to + 1. Negative NDVI values typically correspond to water, snow, or cloud cover. Bare soil or rock surfaces yield values near 0. Positive NDVI values are associated with vegetation, with higher values indicating denser, healthier vegetation cover.

2.2.2. Normalized Difference Built-up Index

The Normalized Difference Built-up Index (NDBI) is a remote sensing metric used to delineate urban built-up regions, including all anthropogenic structures such as residential, industrial, and commercial developments. This metric utilizes the reflectance properties of constructed surfaces in urban areas in the shortwave infrared (SWIR) relative to the near-infrared (NIR). Table 4 summarizes the spectral characteristics of these bands.

Table 4
Landsat spectral bands used for NDBI calculation

Landsat Sensor	SWIR Band	NIR Band	Wavelength Range (μm)
Landsat 5 TM	Band 5	Band 4	SWIR: 1.55–1.75; NIR: 0.76–0.90
Landsat 7 ETM+	Band 5	Band 4	SWIR: 1.55–1.75; NIR: 0.77–0.90
Landsat 8 OLI	Band 6	Band 5	SWIR: 1.57–1.65; NIR: 0.85–0.88
NDBI is given by			

$$NDBI = \frac{SWIR-NIR}{SWIR+NIR}$$ (Eq. 2)

where SWIR and NIR denote reflectance in the shortwave infrared and near-infrared bands, respectively. NDBI values range from − 1 to + 1. Positive NDBI values (> 0) are typically associated with urban built-up areas, whereas negative values (< 0) are associated with non-built urban features such as vegetation, water bodies, or bare soil.

2.3. Land Surface Temperature Inversion

Land Surface Temperature (LST) inversion is the methodology for deriving surface temperature from satellite sensor radiance data. This process involves three principal stages: (i) the conversion of digital numbers (DN) to spectral radiance, (ii) the transformation of radiance into brightness temperature, and (iii) the correction for land surface emissivity to precisely estimate surface temperature.

The first step converts the DN values to spectral radiance using the radiometric rescaling factors provided in the metadata file (MTL):

$L_\lambda = M_L \times Q_{cal} + A_L$

where L_λ is the spectral radiance (W/(m²·sr·μm)), M_L and A_L are the band-specific multiplicative and additive rescaling factors, and Q_{cal} is the DN value.

Brightness temperature (BT) was then calculated using the thermal constants K_1 and K_2 (specific to each Landsat sensor):

$$BT = \frac{k_2}{ln\left(\frac{k_1}{L_\lambda} + 1\right)} - 273 \cdot 15$$

where *BT* is the at-satellite brightness temperature in °C.

Finally, LST was estimated by applying emissivity correction using the NDVI-based approach:

$$LST = \frac{BT}{1 + \left(\frac{\lambda\, xBT}{\rho}\right) ln\epsilon}$$

where λ is the wavelength of emitted radiance (11.5 μm for Landsat TIR), $\rho = h \times c/\sigma$ (with h as Planck's constant, c as the speed of light, and σ as the Boltzmann constant), and ε is the land surface emissivity derived from NDVI thresholds. Table 5 summarizes the spectral characteristics of the thermal bands used for LST retrieval.

Table 5
Landsat thermal bands used for LST retrieval

Landsat Sensor	Thermal Band(s)	Wavelength Range (μm)
Landsat 5 TM	Band 6	10.40–12.50
Landsat 7 ETM+	Band 6 (6L, 6H)	10.40–12.50
Landsat 8 OLI/TIRS	Band 10, Band 11	10.60–11.19; 11.50–12.51

2.3.1. LST Trend Analysis

Trend analysis of Land Surface Temperature (LST) was conducted using multitemporal remote sensing imagery covering the period from 1992 to 2023. LST values were obtained for both mid-summer and late-summer. To eliminate variability in LST caused by seasonal fluctuations, standardized LST values were used for trend analysis. Comparable transformations were also applied to NDVI and NDBI values to facilitate comparison of trends over 31 years (three decades) regarding urban greening and green infrastructure development initiatives within the city. The standardization of LST values was performed using a Z-score transformation, as outlined below.

$$Z = \frac{X - \mu}{\sigma}$$

where X is the observed value, μ is the mean, and σ is the standard deviation.

An analysis of trends in Land Surface Temperature (LST), Normalized Difference Vegetation Index (NDVI), and Normalized Difference Built-up Index (NDBI) was conducted using simple linear regression, with the fitted regression line. This regression line quantifies the direction, magnitude, and significance of temporal changes in LST, NDVI, and NDBI. The Beta coefficient (β_1), or slope, indicates whether the trends of these variables are increasing or decreasing. A positive β_1 denotes an increasing trend over time, whereas a negative β_1 indicates a decreasing trend. Larger absolute values of β_1 correspond to a greater rate of change. The coefficient of determination (R^2) reflects the strength of the trend and the explanatory power of the variable 'time,' while p-values assess the reliability and statistical significance of this trend. The model's optimal-fit line is typically represented as:

$$Y = \beta_0 + \beta_1 X + \varepsilon$$

Where β_0 is the standardized values of LST, NDVI, and NDBI in the reference starting year 1992; β_1 represents the rate of change (trend slope) of standard LST, NDVI, and NDBI values, while ε denotes the error term.

2.4. Validating the Accuracy of LST Retrieval

The accuracy of the Land Surface Temperature (LST) inversion results was initially evaluated using theoretically established relationships with NDVI and NDBI. According to the theory, LST values are positively correlated with NDBI and negatively correlated with NDVI. A similar methodology has been employed in previous studies (e.g., Alfraihat et al., 2016; Estoque et al., 2017; Zhou et al., 2014). Consequently, the ArcGIS Pro random point generator was used to generate fifty points within the municipal boundaries. The multi-point extraction algorithm was used to extract LST, NDVI, and NDBI values at each randomly selected location. Lastly, scatter plots and Pearson correlation analysis were conducted to validate the relationships among the extracted values of LST, NDVI, and NDBI, using metrics such as the correlation coefficient (r) and the sign of the Beta coefficient (β_1), or slope.

Second, the accuracy of the Land Surface Temperature (LST) inversion result is evaluated using in situ air temperature measurements. Research has demonstrated that satellite-derived land surface temperature and near-surface air temperature are highly correlated (e.g., Ermida et al., 2020; Li et al., 2013). Furthermore, LST and air temperature, often regarded as proxies for land-use and land-cover skin temperature, are distinct parameters, with ambient air temperature typically cooler during the day and warmer at night (Ermida et al., 2020). The validation of LST inversion accuracy was performed based on these well-established, strong, and distinct relationships.

3. Results

3.1. Spatiotemporal Dynamics of Land Surface Temperature in Chicago (1992–2023)

Figure 1 presents the spatiotemporal distribution of land surface temperature (LST) in Chicago over the study period (1992–2023), revealing consistent intra-urban temperature variability across years. Accordingly, LST values are spatially dynamic, with the northwestern, northern, western, and southwestern parts of the city exhibiting higher values than the far northern and far southern sides. The LST values in the far southwestern, southern, and central parts of the city were somewhere in between. These spatial dynamics are consistent over the years and throughout the summer, and this pattern is examined.

Mid-summer LST values for Chicago range from a minimum of 20.43°C in 1995 to a maximum of 51.35°C in 2006. Meanwhile, the late-summer LST values ranged from a minimum of 16.68°C in 1992 to a maximum of 47.82°C in 2005. In general, the average mid-summer LST values were 32.22 ± 3.87°C in 1995, 41.52 ± 4.24°C in 2006, 29.48 ± 2.37°C in 2014, and 38.47 ± 3.68°C in 2023, indicating year-to-year variability. Similarly, the average late-summer LST values were 24.27 ± 2.49°C in 1992, 39.17 ± 3.72°C in 2005, 28.6 ± 2.55°C in 2014, and 32.98 ± 3.05°C in 2023, again highlighting annual fluctuations.

The average LST in mid-summer (mid-July to early August) is higher than in late summer (late August and September), as expected. The average summer LST was 35.42 ± 3.54°C, compared with late-summer values of 31.25 ± 2.95°C. LST showed greater variability in late summer, as indicated by the standard deviation, than in mid-summer. The most variable LST values across years occurred in 2006 (SD = 4.24°C) and 2023 (SD = 3.68°C), which also correspond to the hottest surface temperature years. Similarly, the most variable late-summer LST values across years were in 2005 (SD = 4.24°C) and 2023 (SD = 3.68°C), again coinciding with years of hotter late-summer surface temperatures.

3.2. The LST Trend analysis and controls

Figure 2 shows trends in LST, NDBI, and NDVI for Chicago over more than three decades, derived from multitemporal Landsat imagery. It also shows trends in air temperature (°C) for Chicago, as recorded by the Midway Airport station during the satellite's overpass. Accordingly, even if the year-to-year anomalies of the LST values were observed in Fig. 1, there is a consistent trend in the direction of LST value changes. The city’s LST showed an increasing trend over time at a rate of $\beta = 0.03$. However, this increasing trend in LST values over time is not consistent with the city’s land-use and land-cover changes (Fig. 2). According to Fig. 2, during the same period, the city’s NDBI (i.e., built-up areas) values showed a decreasing trend, while the NDVI (i.e., urban greening) values showed an increasing trend over the three decades. The NDBI values decreased at a rate of $\beta = 0.015$, while the NDVI values increased at a rate of $\beta = 0.03$, perhaps reflecting the city’s urban greening efforts, which include transforming vacant lots, implementing green alleys, and installing green roofs.

Given the directional trends toward decreasing built-up areas and increasing urban greening (UHI mitigation strategies), LST values are expected to decrease. Instead, the observed increase in LST over time, despite increases in NDVI and decreases in NDBI, suggests a dominant confounding factor, as evidenced by air temperature values (Fig. 2). During the same period, Chicago’s air temperature

increased at a rate (β = 0.04) comparable to that of NDVI (β = 0.04), suggesting a possible driver of the directional LST increase despite the city's mitigation efforts.

3.3. Verifying the Accuracy of LST Retrieval

3.3.1. The LST, NDVI, and NDBI Relationships with Multitemporal Landsat Imagery

Figure 3 illustrates the relationships among LST, NDVI, and NDBI using multitemporal Landsat imagery from mid- and late summer. The results show that NDVI and NDBI exhibit a strong negative correlation (i.e., R^2 = 0.65–0.86), indicating that as built-up areas increase in the city, greenness decreases. These NDVI-NDBI relationships remained consistent across years (1995, 2006, 2014, 2023) at the time of analysis. Similarly, the relationship between LST and NDVI was negative, suggesting that increases in the city's urban greening are associated with decreases in LST values. Although the LST-NDVI relationships were weaker (R^2 = 0.04–0.18), they remained consistent across years, regardless of the summer season.

Conversely, the relationship between LST and NDBI was positive, indicating that increases in citywide built-up areas are associated with higher LST values. However, the LST-NDBI relationship was weaker (R^2 = 0.08–0.28). The direction of the relationship between LST and NDBI, as verified in this study, aligns with established theoretical relationships. Similarly, the inverse relationships between LST and NDVI, and between NDVI and NDBI, support the known theoretical relationships among these variables. Nonetheless, the stronger association between LST and NDBI compared to LST and NDVI may serve as a reminder that thoughtful urban design is a more effective solution to the UHI phenomenon than mitigation strategies implemented later through urban greening.

3.3.2. Correlation Between Ambient Air Temperature and Land Surface Temperature

Figure 4 shows the relationship between LST values from multitemporal Landsat images (1992–2023) and ambient air temperature recorded at an in-situ station during satellite overpasses in mid- and late-summer. The LST values consistently tracked the in situ atmospheric temperature during both periods. In mid-summer, the citywide average LST was about 37°C in 1992 and increased to nearly 51°C by 2006. The LST then decreased to 33°C in 2014 before rising again to around 43°C in 2023. Meanwhile, the ambient air temperature ranged from roughly 23°C in 1992 to 34°C in 2006, dipped to 29°C in 2014, and was about 31°C in 2023, closely following the LST trends. The dynamics of late summer were similar. The citywide average late-summer LST started at 29°C in 1995, then increased to 48°C in 2005. It was 23°C in 2014 and 38°C in 2023. During the same period, the ambient air temperature was 19°C, 28°C, 23°C, and 24°C in 1995, 2005, 2014, and 2023, respectively, again closely following the LST trends.

During both summer periods, LST values were consistently higher than the ambient air temperature across all observed years. On average, mid-summer LSTs were about 12°C higher than the ambient air

temperature, while late-summer LSTs exceeded it by approximately 13°C. The higher LST readings compared to air temperature support established theories of how the land surface and atmosphere interact with incoming solar radiation. While the atmosphere is often transparent to shortwave solar radiation, Earth's surface absorbs it. This absorbed radiation is converted into thermal (heat) radiation and is emitted into the surrounding air through conduction and convection. Therefore, since the land surface primarily influences air temperature, the pattern shown in Fig. 4 confirms this relationship, substantiating the accuracy of the computed land surface temperature inversions.

4. Discussion

4.1. Urban Heat Patterns and Land-Cover Relationships in Chicago

Over the past 30 years, land surface temperatures (LST) in Chicago have shown consistent spatiotemporal variation. Spatially, LST varies across the city, with the northwestern, northern, western, and southwestern sides experiencing higher temperatures than the far northern and far southern sides. Temporally, mid-summer LST values are generally higher than late-summer temperatures, with substantial year-to-year variability. The hottest and most variable surface temperature years occurred in the mid-2000s and again in 2023, indicating episodic periods of intensified urban heat. Previous studies have demonstrated that urban heat patterns typically exhibit strong spatiotemporal variation influenced by land-cover composition, urban morphology, and surface characteristics (Li et al., 2019; Zhao et al., 2014). Densely built environments with limited vegetation often experience higher surface temperatures, whereas areas with greater vegetation cover or open spaces tend to remain relatively cooler (Peng et al., 2012; Tan et al., 2023; Zhou et al., 2014). Similar spatial patterns of urban heat have also been reported in several metropolitan regions, where variations in urban structure and land cover significantly influence surface temperature distribution. In Chicago specifically, previous research has documented extreme heat events and their impacts on urban populations, including the severe 1995 heat wave, which highlighted the city’s vulnerability to extreme temperatures (IPCC, 2021; Klinenberg, 2002). While many previous studies focused on short-term observations or specific extreme events, this study provides a long-term perspective by analyzing more than three decades of multitemporal Landsat observations from 1992 to 2023. This extended temporal analysis allows for a clearer understanding of both long-term trends and episodic variations in Chicago’s urban thermal environment.

Over the past three decades (1992–2023), multitemporal Landsat observations show that Chicago’s land surface temperature (LST) has steadily increased, despite year-to-year variability. During the same period, the built-up area index (NDBI) declined while the urban vegetation index (NDVI) increased, reflecting urban greening initiatives such as green roofs, green alleys, and the conversion of vacant lots. The continued rise in LST, despite these mitigation efforts, appears largely driven by rising air temperatures, suggesting that broader climatic warming may be overriding local land-cover improvements, consistent with recent findings that global warming amplifies urban heat beyond local

mitigation capacity (IPCC, 2021; Perkins-Kirkpatrick & Lewis, 2020). Previous studies have consistently shown that vegetation plays a critical role in regulating urban surface temperatures. Vegetated surfaces typically reduce surface temperatures through shading and evapotranspiration, while impervious built-up surfaces tend to absorb and retain heat, contributing to higher urban temperatures (Perkins-Kirkpatrick & Lewis, 2020; Santamouris, 2015; Zhao et al., 2014). Several remote sensing studies have also reported negative relationships between vegetation indices and land surface temperature, highlighting the cooling effects of urban greenery (Li et al., 2019; Li et al., 2024; Zhou et al., 2014). In response to these findings, many cities have implemented urban greening initiatives to mitigate the urban heat island effect (Bowler et al., 2010; Santamouris, 2015). Chicago has similarly promoted green infrastructure strategies, including green roofs and urban greening programs, to improve urban environmental conditions and reduce surface temperatures (Tan et al., 2023). The results of this study provide an important extension to previous research by demonstrating that increasing vegetation alone may not fully offset rising surface temperatures, despite evidence that urban vegetation significantly improves microclimatic conditions (Chun & Guldmann, 2018; Fadhil et al., 2023; Tan et al., 2023). This highlights the complex interaction between local land-cover changes and larger-scale climate processes, as recent studies show that climate change-driven warming can offset the localized cooling benefits of urban greening (Tan et al., 2023; Zhao et al., 2014).

Multitemporal Landsat analysis shows a strong negative relationship between vegetation (NDVI) and built-up areas (NDBI), indicating that increased urban development reduces urban greenness. Land Surface Temperature (LST) was also negatively related to NDVI and positively related to NDBI, confirming that greener areas tend to cool while built-up surfaces contribute to higher urban heat. This finding aligns with recent studies showing that increasing impervious surfaces and urban expansion significantly intensify urban heat island effects (Yee & Kaplan, 2022). Across 1992–2023, ambient air temperature closely tracked LST, indicating that land-surface heating is a potential source of atmospheric heating, consistent with studies linking surface heating to atmospheric temperature dynamics (Tan et al., 2023; Li et al., 2019; Voogt & Oke, 2003). Satellite-derived indices show that NDVI typically exhibits a negative correlation with LST, reflecting the cooling effect of vegetation through shading and evapotranspiration (Bowler et al., 2010; Zhou et al., 2015). An ecological evaluation of the urban heat island in Chicago, conducted by Alfraihat et al. (2016), demonstrated that relationships among LST, NDVI, and NDBI can be used to assess the ecological condition of urban thermal environments. Using the Urban Thermal Field Variance Index (UTFVI), their study found that approximately 25% of Chicago experienced ecologically unfavorable UHI conditions despite the cooling influence of urban parks and Lake Michigan. These findings emphasize the importance of vegetation and ecological balance in regulating urban thermal environments. While previous studies primarily focused on ecological evaluation of urban heat island conditions, the present study extends this understanding by examining long-term relationships among vegetation, built-up areas, land surface temperature, and atmospheric temperature over more than three decades (1992–2023).

4.2. Implications for Climate-Resilient Urban Planning

The findings of this study have important implications for developing climate-resilient cities. The long-term increase in land surface temperature observed in Chicago underscores the growing challenge of urban heat in the context of global climate change. Although urban greening initiatives have increased vegetation cover in several parts of the city, the continued rise in surface temperatures suggests that local mitigation strategies alone may not be sufficient to offset broader climate warming. The observed relationships among vegetation (NDVI), built-up areas (NDBI), and land surface temperature underscore the critical role of urban land-cover management in regulating urban thermal environments. Areas with higher vegetation density consistently showed lower surface temperatures, whereas built-up areas exhibited higher thermal intensity. These findings suggest that expanding the urban tree canopy, protecting green spaces, and integrating nature-based solutions, such as green roofs, urban parks, and urban green corridors, could play a significant role in reducing urban heat exposure. More broadly, the results highlight the importance of integrating climate-sensitive urban planning strategies into long-term development policies. By identifying spatial patterns and long-term trends in urban heat, this research provides valuable information for urban planners and policymakers seeking to design more climate-resilient and thermally sustainable cities.

4.3. Limitations and Future Research

Despite its contributions, this study has several limitations. First, the analysis relies primarily on satellite-derived land surface temperature, which reflects surface thermal conditions rather than the near-surface air temperature experienced by urban residents. Although daily average air temperature data from the Midway Airport station via Weather Underground were included for comparison, these data are limited to a single station and may not fully capture spatial variability in urban air temperature across the city. Second, the study uses Landsat imagery at fixed time intervals, which may not fully capture variability on shorter time scales. Third, other factors, such as building density, urban morphology, and socioeconomic conditions, were not explicitly incorporated into the analysis. Therefore, future research should address these limitations by integrating higher-resolution remote sensing data, continuous meteorological observations, and detailed urban morphology datasets. Incorporating building density and socioeconomic variables would provide a more comprehensive understanding of urban heat dynamics. Such approaches would improve the ability to identify vulnerable areas and support more effective urban planning and climate adaptation strategies.

5. Conclusion

This study presents a comprehensive, multi-decadal assessment of urban heat dynamics in Chicago from 1992 to 2023. It employs multitemporal satellite-derived indices, including land surface temperature (LST), vegetation (NDVI), and built-up areas (NDBI), to evaluate trends and drivers of the Urban Heat Island (UHI) phenomenon. The findings demonstrate an increase in LST over the period. Mid-summer LSTs exceed those in late summer, with notable interannual variability, especially during peak heat years such as 2005, 2006, and 2023. The spatial distribution underscores the inherently uneven nature of urban heat in Chicago, highlighting crucial environmental justice considerations and

emphasizing the need for targeted interventions, as populations in high-heat zones may face disproportionate exposure to heat-related risks.

Furthermore, the findings demonstrate that Chicago's Land Surface Temperature (LST) shows a consistent upward trend throughout the study period, despite decreases in built-up areas and increases in vegetation. This trend is likely influenced by rising ambient air temperatures, which appear to outweigh the effects of mitigation efforts such as urban tree planting, green roofs, and the redevelopment of impervious surfaces. The ongoing increase in LST supports the argument that urban heat is not solely a consequence of land-cover changes but also arises from its impact on regional and global climate dynamics. Consequently, in addition to urban greening initiatives, efforts to mitigate the Urban Heat Island (UHI) effect in Chicago should adopt a more comprehensive strategy. This strategy should incorporate land-use planning to increase surface albedo; enhance climate adaptation and resilience by deploying evenly distributed green infrastructure; adopt architectural designs that mitigate urban canyon effects and promote airflow; and implement energy management practices to reduce anthropogenic heat emissions.

Despite its contributions, this study is limited by its reliance on satellite-derived Land Surface Temperature (LST) and a limited set of in situ air temperature measurements, as well as by the omission of detailed socioeconomic and urban morphological variables. Future research should integrate high-resolution remote sensing data, expanded meteorological observations, and socio-environmental indicators to foster a more comprehensive understanding of urban heat dynamics and to support the development of more effective, climate-resilient urban planning strategies.

Declarations

Conflict of Interest

The authors declare that they have no known conflicts of interest that could have appeared to influence the work reported in this manuscript

Funding

This study was supported by the Community Research on Climate and Urban Science (CROCUS) an initiative led by the U.S. Department of Energy's Argonne National Laboratory under grant number DE-SC0023298.

Data Availability Statement

The datasets presented in this article are available upon reasonable request from the authors. Requests to access the datasets should be directed to tgala@csu.edu

Ethics approval and consent to participate

Not applicable

Consent for publication

Not applicable

Materials availability

Not applicable.

Code availability

Not applicable

Author Contribution

In the research article, Ms. Alam is the first author, as she led the research scope and problems, the sampling design, data acquisition, preprocessing, analysis, and a partial write-up. Dr. Gala is the corresponding author. He guided and led the definition of the research scope and problems, the design of the research approach, the analyses and interpretations of the research results, and the writing of the manuscript. Dr. Block contributed to grant acquisition, project administration, manuscript review, and manuscript editing. Ms. Haile contributed valuable literature to support the interpretation of the research results, reviewed and edited the manuscript, and prepared the manuscript. Mr. Bhattarai contributed to the organization, formatting, writing, reviewing, and editing of the manuscript.

Acknowledgement

The authors are grateful to anonymous reviewers for this manuscript. Additionally, the Geographic Information Systems (GIS) laboratory at Chicago State University (CSU) provides software, and the Environmental Systems Research Institute (ESRI) provides technical support for the software.

Data Availability

The data supporting the findings of this study are openly available. The Satellite data was acquired from the Earth Resources Observation and Science (EROS) Center operated by the U.S. Geological Survey (USGS) (https://earthexplorer.usgs.gov). The hourly Temperature data were obtained from the National Weather Service (https://www.weather.gov/wrh/Climate?wfo=lot).

Acknowledgement

The authors are grateful to anonymous reviewers for this manuscript. Additionally, the Geographic Information Systems (GIS) laboratory at Chicago State University (CSU) provides software, and the Environmental Systems Research Institute (ESRI) provides technical support for the software.

References

1. Aghazadeh, F., Samadi, M., Cheval, S., & Moshiri, S. (2025). Impacts of land use, vegetation, and air pollution on surface urban heat island spatiotemporal dynamics: Tehran as a case study. *International Journal of Environmental Science and Technology, 22*, 14607–14633. https://doi.org/10.1007/s13762-025-06561-8
2. Alfraihat, R., Mulugeta, G., & Gala, T. S. (2016). Ecological evaluation of urban heat island in Chicago city, USA. *Journal of Atmospheric Pollution, 4*(1), 23–29. https://doi.org/10.12691/jap-4-1-3
3. Anderson, G. B., & Bell, M. L. (2010). Heat waves in the United States: Mortality risk during heat waves and effect modification by heat wave characteristics in 43 USA communities. *Environmental Health Perspectives, 119*(2). https://doi.org/10.1289/ehp.1002313
4. Boakye, L. (2019). The Use of Remote Sensing and GIS for Monitoring Urban Growth: The Case of Addis Ababa, Ethiopia. Chicago State University. https://doi.org/10.13140/RG.2.2.15870.41280
5. Bowler, D. E., Lisette, B. A., Knight, T. M., & Pullin, A. S. (2010). Urban greening to cool towns and cities: A systematic review of the empirical evidence. *Landscape and Urban Planning, 97*(3), 147–155. https://doi.org/10.1016/j.landurbplan.2010.05.006
6. Chen, K., Boomsma, J., & Holmes, H. A. (2023). A multiscale analysis of heatwaves and urban heat islands in the western U.S. during the summer of 2021. *Scientific Reports, 13*, 9570. https://doi.org/10.1038/s41598-023-35621-7
7. Chun, B., & Guldmann, J.-M. (2018). Impact of greening on the urban heat island: Seasonal variations and mitigation strategies. *Computers, Environment and Urban Systems, 71*, 165–176. https://doi.org/10.1016/j.compenvurbsys.2018.05.006
8. Ebi, K. L., Capon, A., Berry, P., Broderick, C., de Dear, R., Havenith, G., Honda, Y., Kovats, R. S., Ma, W., Malik, A., Morris, N. B., Nybo, L., Seneviratne, S. I., Vanos, J., Jay, O., et al. (2021). Hot weather and heat extremes: Health risks. *The Lancet*, 398(10301), 698–708. https://doi.org/10.1016/s0140-6736(21)01208-3
9. Ermida, S. L., Trigo, I. F., Hulley, G., & DaCamara, C. C. (2020). A multi-sensor approach to retrieve emissivity angular dependence over desert regions. *Remote Sensing of Environment, 237*, 111559. https://doi.org/10.1016/j.rse.2019.111559
10. Estrada, F., Botzen, W. J. W., & Tol, R. S. J. (2017). A global economic assessment of city policies to reduce climate change impacts. *Nature Climate Change, 7*(6), 403–406. https://doi.org/10.1038/nclimate3301
11. Estoque, R. C., Murayama, Y., & Myint, S. W. (2017). Effects of landscape composition and pattern on land surface temperature: An urban heat island study in the megacities of Southeast Asia. *Science of the Total Environment, 577*, 349–359. https://doi.org/10.1016/j.scitotenv.2016.10.195

12. Fadhil, M., Hamoodi, M. N., & Ziboon, A. R. T. (2023). Mitigating urban heat island effects in urban environments: Strategies and tools. *IOP Conference Series: Earth and Environmental Science, 1129*, 012025. https://doi.org/10.1088/1755-1315/1129/1/012025
13. Friehat, T., Mulugeta, G., & Gala, T. S. (2015). Modeling urban sprawls in Northeastern Illinois. *Journal of Geosciences and Geomatics*, 3(5), 133–141. https://doi.org/10.12691/jgg-3-5-4
14. Grimmond, C. S. B., & Oke, T. R. (1999). Aerodynamic properties of urban areas derived from analysis of surface form. *Journal of Applied Meteorology, 38*, 1262–1292. https://doi.org/10.1175/1520-0450(1999)038%3C1262:APOUAD%3E2.0.CO;2
15. Habila, M. (2018). Monitoring Land Use/Land Cover Change Using Remote Sensing Data and Geographical Information Sciences (GIS): A Case Study of Abuja, Nigeria (Master's thesis, Chicago State University). https://doi.org/10.13140/RG.2.2.31463.98723
16. Hoffman, J. S., Shandas, V., & Pendleton, N. (2020). The effects of historical housing policies on resident exposure to intra-urban heat: A study of 108 US urban areas. *Climate, 8*(1). https://doi.org/10.3390/cli8010012
17. Im, E. S., Pal, J. S., & Eltahir, E. A. B. (2017). Deadly heat waves are projected in the densely populated agricultural regions of South Asia. *Science Advances, 3*(8). https://doi.org/10.1126/sciadv.1603322
18. Intergovernmental Panel on Climate Change. (2021). *Climate change 2021: The physical science basis*. Cambridge University Press. https://doi.org/10.1017/9781009157896
19. Janků, Z., Geletič, J., Lehnert, M., & Dobrovolný, P. (2024). The increase in urban heat due to global warming can be significantly affected by the structure of land use and land cover. *International Journal of Climatology, 44*(15), 5381–5397. https://doi.org/10.1002/joc.8642
20. Klinenberg, E. (2002). *Heat wave: A social autopsy of disaster in Chicago*. University of Chicago Press.
21. Lee, J., Berkelhammer, M., Wilson, M. D., Love, N., & Cintron, R. (2024). Urban land surface temperature downscaling in Chicago: Addressing ethnic inequality and gentrification. *Remote Sensing, 16*(9), 1639. https://doi.org/10.3390/rs16091639
22. Lewis, P., Gómez-Dans, J., Kaminski, T., Settle, J., Quaife, T., Gobron, N., Styles, J., & Berger, M. (2012). An Earth Observation Land Data Assimilation System (EO-LDAS). *Remote Sensing of Environment, 120*, 219–235. https://doi.org/10.1016/j.rse.2011.12.027
23. Li, Z.-L., Tang, B.-H., Wu, H., Ren, H., Yan, G., Wan, Z., … Sobrino, J. A. (2013). Satellite-derived land surface temperature: Current status and perspectives. *Remote Sensing of Environment, 131*, 14–37. https://doi.org/10.1016/j.rse.2012.12.008
24. Li, D., Liao, W., Rigden, A. J., Liu, X., Wang, D., Malyshev, S., & Shevliakova, E. (2019). Urban heat island: Aerodynamics or imperviousness? *Science Advances, 5*(4), eaau4299. https://doi.org/10.1126/sciadv.aau4299
25. Lokoshchenko, M. A., & Alekseeva, L. I. (2023). Influence of meteorological parameters on the urban heat island in Moscow. *Atmosphere, 14*(3). https://doi.org/10.3390/atmos14030507

26. McKenzie, R. (2022). Assessing the flood hazard and risk of Montego Bay using Geographic Information System-based multicriteria analysis (Master's thesis, Chicago State University). https://doi.org/10.13140/RG.2.2.22586.47048
27. McKenzie, R., & Gala, T. (2023). Likelihoods of Flood Hazards and Risks Using GIS-Based Analytical Hierarchy Process (AHP). *Academic Journal of Environment & Earth Science*, 5(9). https://doi.org/10.25236/AJEE.2023.050902
28. Mengisti, M., Gala, T., & Birru, G. (2021). Environmentally Conscious Least-Cost Multi-Criteria Decision Making for Modeling the Railway Network of Eritrea. *International Journal of Sustainable Development & Planning*. https://doi.org/10.18280/ijsdp.16030
29. Morabito, M., Crisci, A., Guerri, G., Messeri, A., Congedo, L., & Munafò, M. (2021). Surface urban heat islands in Italian metropolitan cities: Tree cover and impervious surface influences. *Science of the Total Environment, 751*, 142334. https://doi.org/10.1016/j.scitotenv.2020.142334
30. Pawlowski, M. E. (2025). Analyzing Air Quality Heterogeneity and Data Deserts in Chicago (Master's thesis, Chicago State University). https://doi.org/10.13140/RG.2.2.13674.02247
31. Pawlowski, M., Gala, T., Bhattarai, A., Alam, S., Block, D., McDonough, M., ... & Muradyan, P. (2026). Disparities in air-quality monitoring stations and $PM_{2.5}$ in Chicago's air quality landscape. *Discover Public Health*, 23(1), 415. https://doi.org/10.1186/s12982-026-01792-7
32. Perkins-Kirkpatrick, S. E., & Gibson, P. B. (2017). Changes in regional heatwave characteristics as a function of increasing global temperature. *Scientific Reports, 7*(1). https://doi.org/10.1038/s41598-017-12520-2
33. Peng, et al. (2012). Surface urban heat island across 419 global big cities. *Environmental Science & Technology, 46*(2). https://doi.org/10.1021/es2030438
34. Sampson, N. R., Gronlund, C. J., Buxton, M. A., Catalano, L., White-Newsome, J. L., Conlon, K. C., Neill, M. S. O., McCormick, S., & Parker, E. A. (2013). Staying cool in a changing climate: Reaching vulnerable populations during heat events. *Global Environmental Change, 23*(2), 475–484. https://doi.org/10.1016/j.gloenvcha.2012.12.011
35. Santamouris, M. (2015). Analyzing the heat island magnitude and characteristics in one hundred Asian and Australian cities and regions. *Science of the Total Environment*. https://doi.org/10.1016/j.scitotenv.2015.01.060
36. Sailor, D. J. (2011). A review of methods for estimating anthropogenic heat and moisture emissions in the urban environment. *International Journal of Climatology, 31*(2). https://doi.org/10.1002/joc.2106
37. Semenza, J. C., McCullough, J. E., Flanders, W. D., McGeehin, M. A., & Lumpkin, J. R. (1999). Excess hospital admissions during the July 1995 heat wave in Chicago. *American Journal of Preventive Medicine, 16*(4), 269–277. https://doi.org/10.1016/S0749-3797(99)00025-2
38. Shahmohamadi, P., Che-Ani, A. I., Maulud, K. N. A., Tawil, N. M., & Abdullah, N. A. G. (2011). The impact of anthropogenic heat on formation of urban heat island and energy consumption balance. *Urban Studies Research, 2011*, 497524. https://doi.org/10.1155/2011/497524

39. Smith, M., Bhattarai, A., Alam, S., Gala, T., Fears, N. S., Berkelhammer, M., ... & Kalo, E. (2026). Neighborhood-Scale Urban Tree Assessment: The Case of Chatham Neighborhood, Chicago. https://doi.org/10.21203/rs.3.rs-9133372/v1
40. Tan, H., Kotamarthi, R., Wang, J., Qian, Y., & Chakraborty, T. C. (2023). Impact of different roofing mitigation strategies on near-surface temperature and energy consumption over the Chicago metropolitan area during a heatwave event. *Science of the Total Environment, 860*, 160508. https://doi.org/10.1016/j.scitotenv.2022.160508
41. U.S. Census Bureau. (2023). *QuickFacts: Chicago city, Illinois*. https://www.census.gov/quickfacts/chicagocityillinois
42. U.S. Environmental Protection Agency. (2002). *Reducing urban heat islands: Compendium of strategies*. https://www.epa.gov/heatislands
43. Voogt, J. A., & Oke, T. R. (2003). Thermal remote sensing of urban climates. *Remote Sensing of Environment, 86*(3), 370–384. https://doi.org/10.1016/S0034-4257(03)00079-8
44. Weng, Q. (2009). Thermal infrared remote sensing for urban climate and environmental studies: Methods, applications and trends. *ISPRS Journal of Photogrammetry and Remote Sensing, 64*(4), 335–344. https://doi.org/10.1016/j.isprsjprs.2009.03.007
45. Wuebbles, D., Angel, J., Petersen, K., & Lemke, A. M. (Eds.). (2021). *An assessment of the impacts of climate change in Illinois*. The Nature Conservancy. https://doi.org/10.13012/B2IDB-1260194_V1
46. Yee, M., & Kaplan, J. O. (2022). Drivers of urban heat in Hong Kong over the past 116 years. *SSRN Electronic Journal*. https://doi.org/10.2139/ssrn.4174745
47. Ziter, C. D., Pedersen, E. J., Kucharik, C. J., & Turner, M. G. (2019). Scale-dependent interactions between tree canopy cover and impervious surfaces reduce daytime urban heat during summer. *Proceedings of the National Academy of Sciences, 116*(15), 7575–7580. https://doi.org/10.1073/pnas.1817561116
48. Zhou, B., Rybski, D., & Kropp, J. P. (2017). The role of city size and urban form in the surface urban heat island. *Scientific Reports, 7*. https://doi.org/10.1038/s41598-017-04242-2
49. Zhao, L., Lee, X., Smith, R. B., & Oleson, K. W. (2014). Strong contributions of local background climate to urban heat islands. *Nature, 511*(7508), 216–219. https://doi.org/10.1038/nature13462
50. Zhou, D., Zhao, S., Zhang, L., Sun, G., Liu, Y. (2015). The footprint of the urban heat island effect in China. *Scientific Reports, 5*. https://doi.org/10.1038/srep11160.

Figures

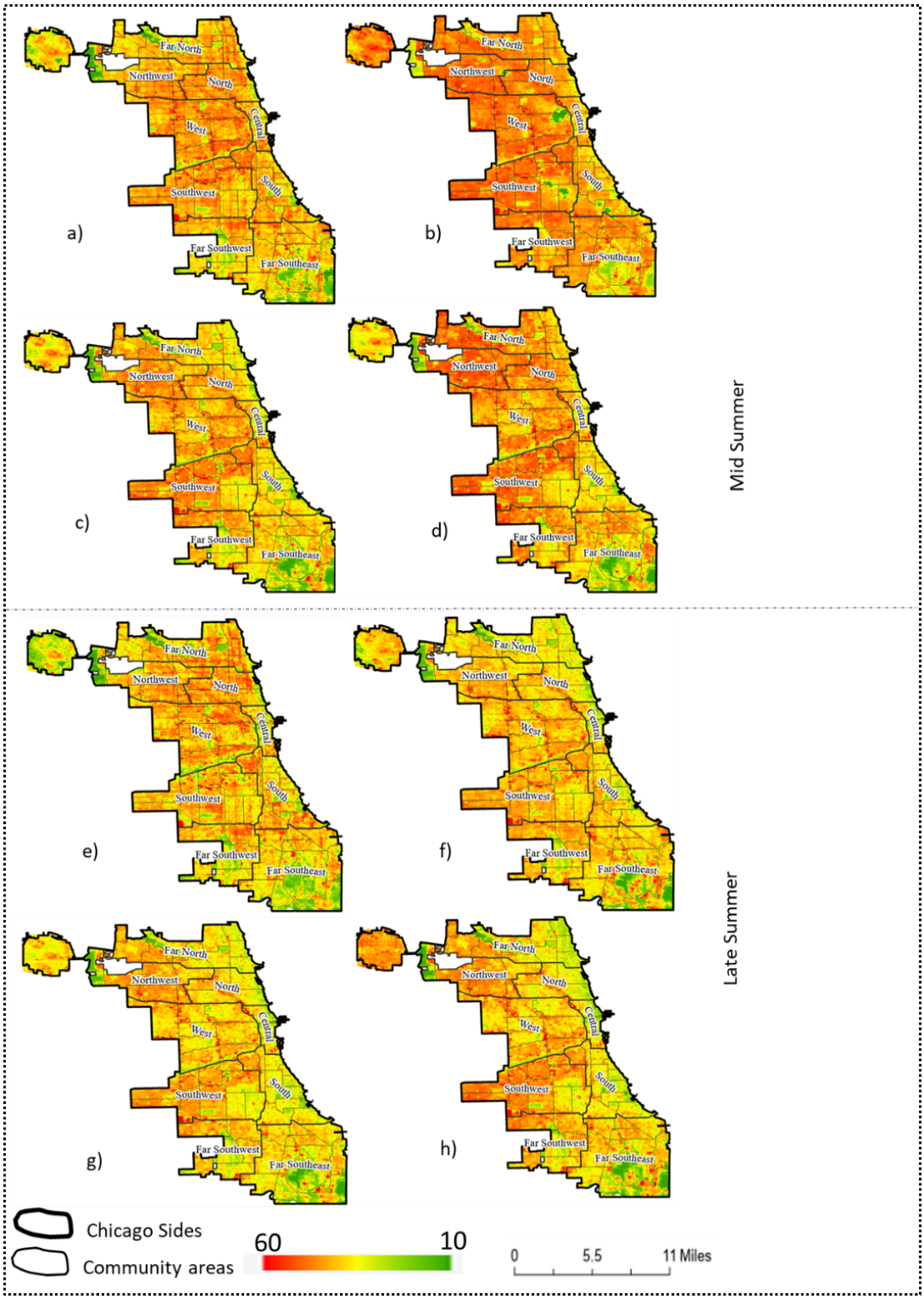


Figure 1

Spatial distribution of LST in Chicago (1992-2023): Mid-summer a) 1995, b) 2006, c) 2014, and d) 2023; Late-summer e) 1992, f) 2005, g) 2014, and h) 2023

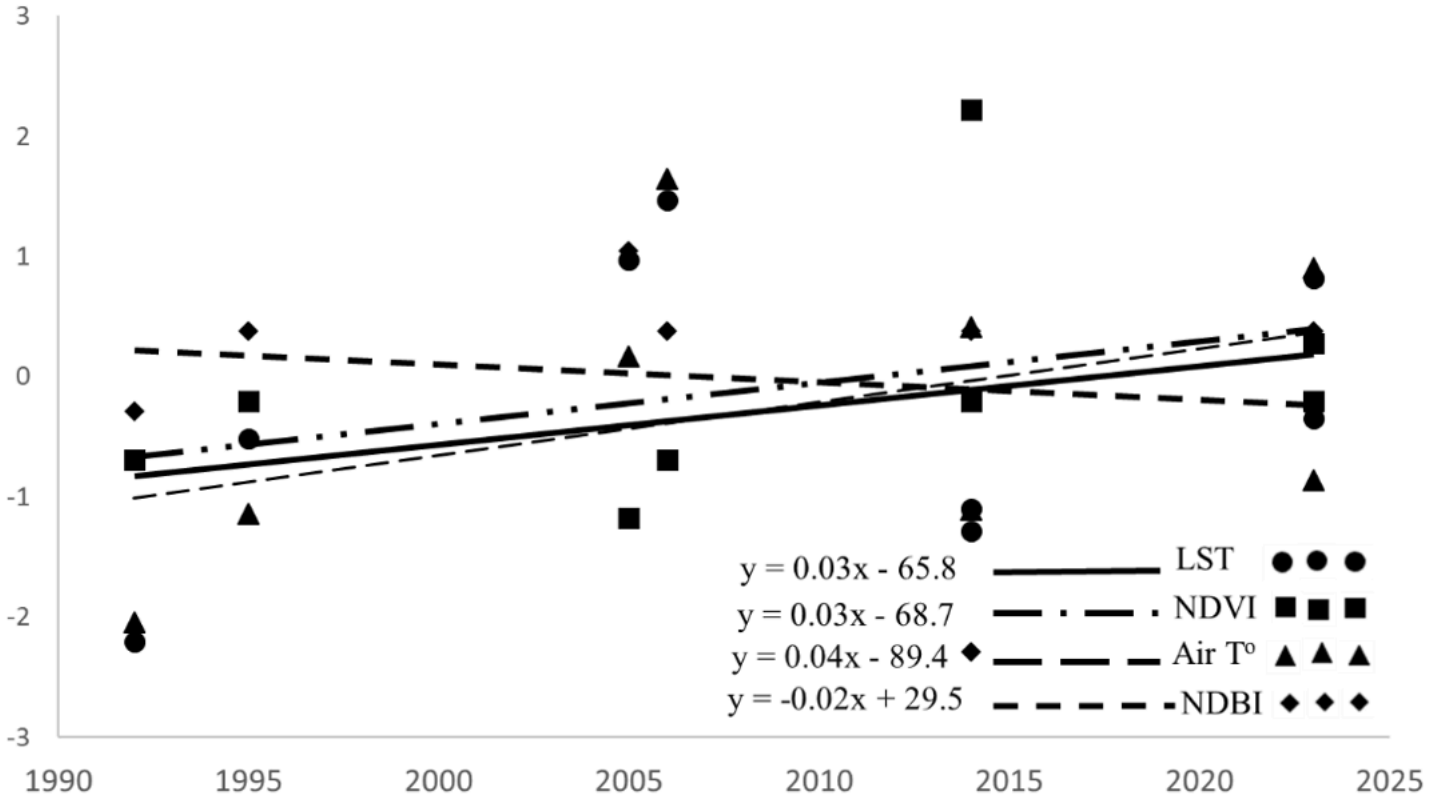


Figure 2

Trend analysis of LST, NDVI, and NDBI values of Chicago

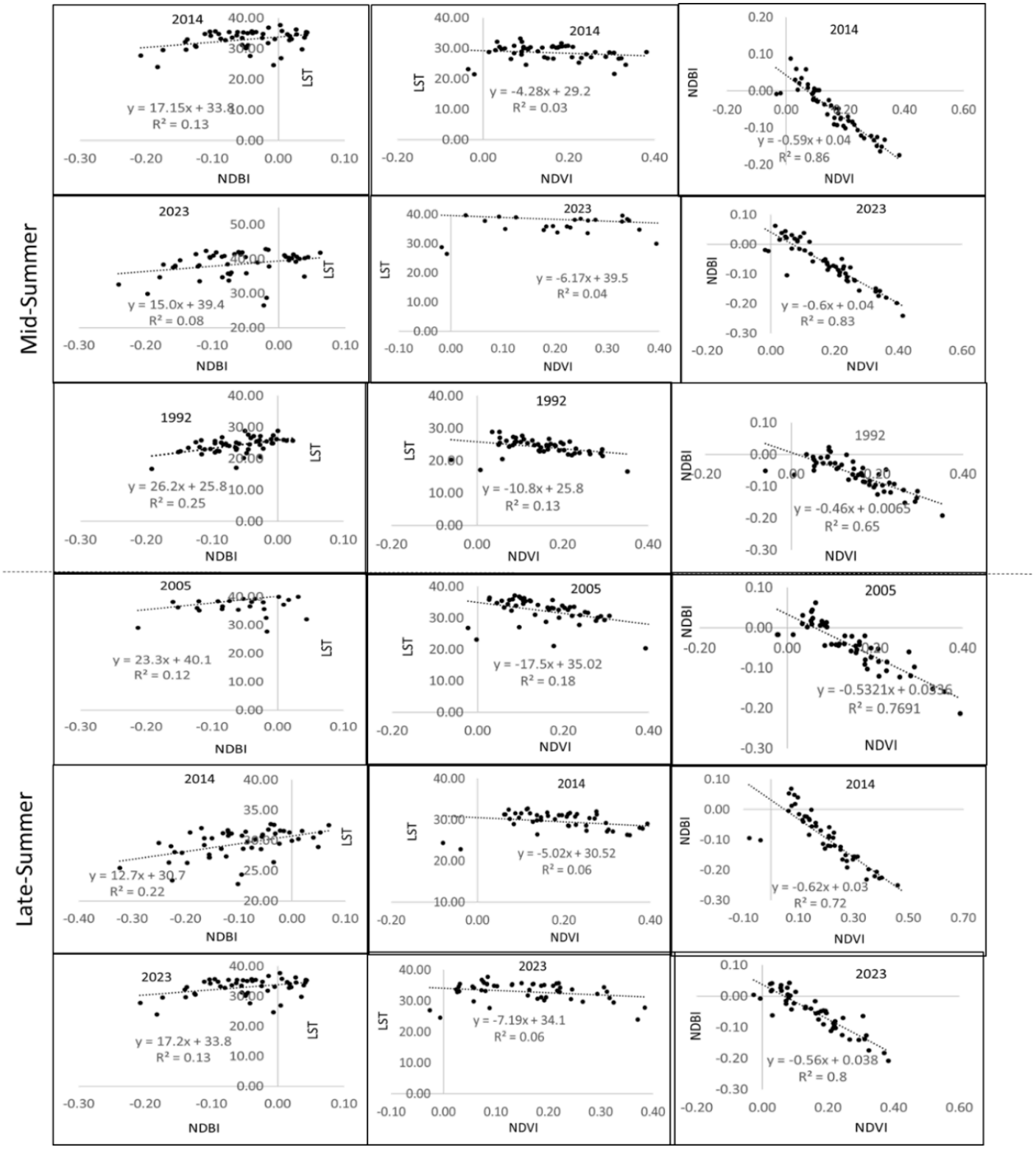


Figure 3

The LST, NDVI, and NDBI Relationships with the mid-and late-summer multitemporal Landsat imagery

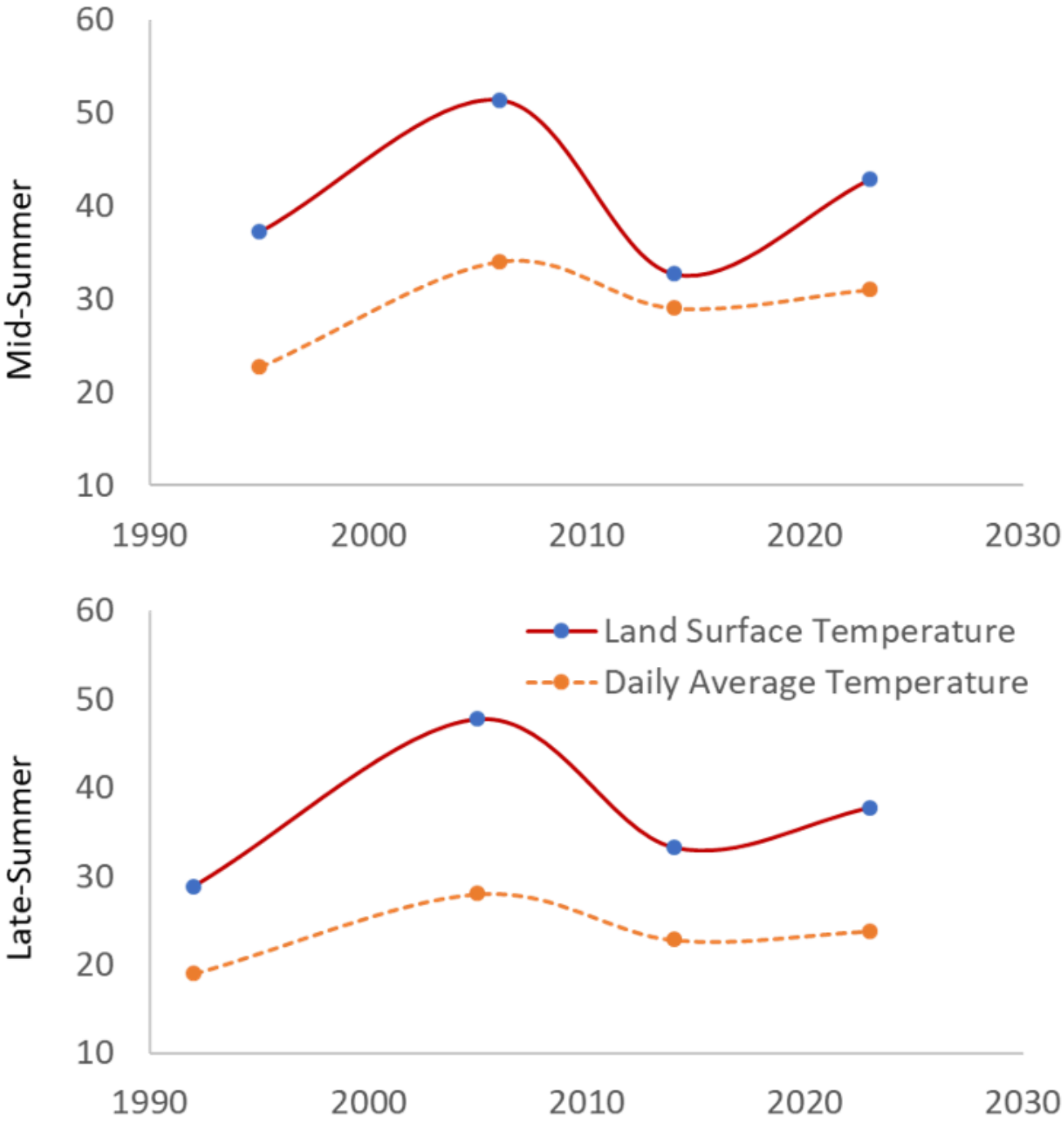


Figure 4

The dynamic mid-and late-summer coupling of the LST values retrieved from the multitemporal Landsat imageries and ambient atmospheric air temperature using the in-situ station